JACS
JOURNAL OF THE AMERICAN CHEMICAL SOCIETY

Article

pubs.acs.org/JACS

Ion Mobility Spectrometry Reveals the Mechanism of Amyloid Formation of Aβ(25−35) and Its Modulation by Inhibitors at the Molecular Level: Epigallocatechin Gallate and *Scyllo*-inositol

Christian Bleiholder,[†] Thanh D. Do,[†] Chun Wu, Nicholas J. Economou, Summer S. Bernstein, Steven K. Buratto, Joan-Emma Shea, and Michael T. Bowers*

Department of Chemistry and Biochemistry, University of California, Santa Barbara, California 93106-9510, United States

Supporting Information

ABSTRACT: Amyloid cascades leading to peptide β-sheet fibrils and plaques are central to many important diseases. Recently, intermediate assemblies of these cascades were identified as the toxic agents that interact with the cellular machinery. The relationship between the transformation from natively unstructured assembly to the β-sheet oligomers to disease is important in understanding disease onset and the development of therapeutic agents. Research on this early oligomeric region has largely been unsuccessful since traditional techniques measure only ensemble average oligomer properties. Here, ion mobility methods are utilized to deduce the modulation of peptide self-assembly pathways in the amyloid-β protein fragment Aβ(25−35) by two amyloid inhibitors (epigallocatechin gallate and *scyllo*-inositol) that are currently in clinical trials for Alzheimer's Disease. We provide evidence that suppression of β-extended oligomers from the onset of the conversion into β-oligomer conformations is essential for effective attenuation of β-structured amyloid oligomeric species often associated with oligomer toxicity. Furthermore, we demonstrate the ease with which ion mobility spectrometry−mass spectrometry can guide the development of therapeutic agents and drug evaluation by providing molecular level insight into the amyloid formation process and its modulation by small molecule assembly modulators.

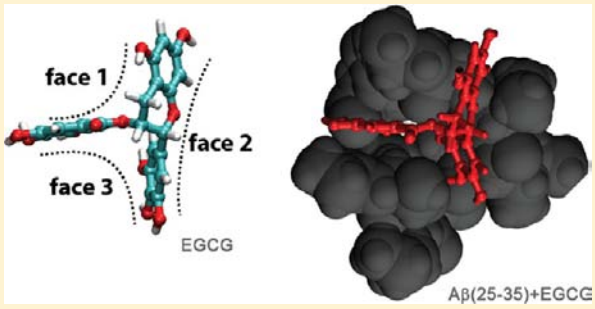

INTRODUCTION

The aberrant deposition of protein plaques is the common histopathological hallmark of amyloid diseases,[1−3] such as Huntington's, Parkinson's, Alzheimer's or type 2 diabetes. Amyloid plaques of distinct diseases differ from each other mainly by the protein deposited and the specific tissues subjected to plaque deposition and degeneration.[1] Experimental evidence[4] indicates that amyloid diseases share a common pathogenic mechanism which attributes a generic toxicity[5,6] to soluble protein oligomers that are transiently populated during amyloid formation.[7−11] A conversion of soluble oligomers from globular conformations into amyloid β-strand structures is postulated to be of central relevance to disease pathogenesis.[1] Thus, protein self-assembly processes that sustain a conformational conversion into amyloid assemblies are considered pathogenic (generalized amyloid cascade hypothesis).[1,5,6,12,13]

One currently highly investigated approach to amyloid disease therapeutics is to directly manipulate the pathogenic protein aggregation process such that the toxic agents are no longer formed.[14−21] Significant progress has been made recently in using ligands to transform pathogenic into benign protein aggregation pathways.[16,18,19,22] Small organic compounds,[23,24] in particular the polyphenol epigallocatechin gallate (EGCG)[16,25−31] or the carbohydrate *scyllo*-inositol,[16,32] were reported to exhibit cytoprotective effects by redirecting fibril formation into unstructured macroscopic aggregates for a number of amyloid forming proteins, and are currently in clinical trials for Alzheimer's disease (AD).[31] Other compounds, especially negatively charged glycosaminoglycans, were found to reduce cytotoxicity by promoting protein assembly into amyloid fibrils.[17,33−39] The particular cytoprotective effects of these compounds appear to be generic in nature and rather independent of the particular protein investigated and specific experimental conditions applied.[16,30,31,36,40]

Attempts to relate cytoprotective effects to changes in aggregate morphology induced by the ligands have been conflicting.[41] For one, cytoprotection is achieved by redirecting protein self-assembly into macroscopically unstructured aggregates,[22,24,28,29,31] but also by accelerating the postulated pathogenic fibrillogenesis pathway.[16,17,35] Significantly, mature aggregates of amyloid-β (Aβ) variants with distinct macroscopic morphologies were found to exhibit an equivalent degree of toxicity,[9] which was attributed to differences in transiently populated oligomers. Furthermore, two aggregation pathways of the amyloid forming protein HypF-N were described that result in similar morphologies of their mature macroscopic aggregates. However, one oligomer type is benign when added

Received: June 19, 2013
Published: October 16, 2013

Scheme 1. Structural Formulas of Aβ(25-35), Epigallocatechin Gallate (EGCG) and *Scyllo*-inositol

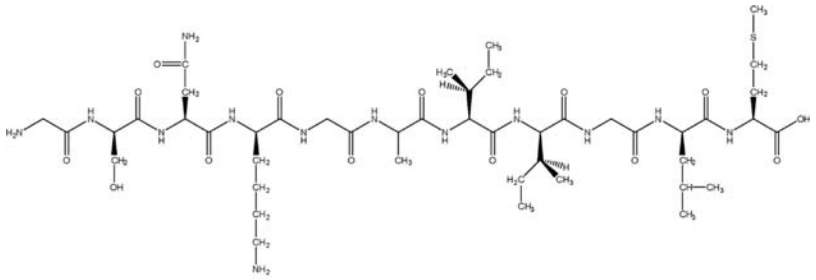

amyloid-$\beta_{25\text{-}35}$ (GSNKGAIIGLM)

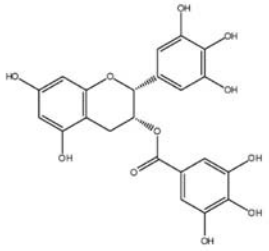

epigallocatechin gallate (EGCG)

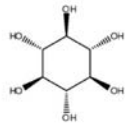

scyllo-inositol

to cell cultures whereas the other is toxic,[42] an observation ascribed to structural differences observed for the corresponding soluble oligomers. These results underline the importance of directly elucidating the morphologies of early, transient soluble oligomers during amyloid formation and thus highlight a strong disconnect between key disease processes and the structural information amenable from bulk measurements of macroscopic aggregates.

Recently[43] we reported on the first direct observation of structural transition processes that occur during the self-assembly of peptides en route to mature aggregates as soluble oligomers grow one monomer at a time using ion mobility spectrometry–mass spectrometry (IMS–MS). In the current work, we apply IMS–MS[10,44−50] to characterize the self-assembly process of Aβ(25–35), an important fragment of the neurologically important Aβ40 and Aβ42 peptides responsible for Alzheimer's Disease.[51] Our intent is to determine the structural implications induced by the ligands epigallocatechin gallate (EGCG) and *scyllo*-inositol on transient, soluble Aβ(25–35) oligomers (see Scheme 1).

EGCG and *scyllo*-inositol are protein assembly modulators currently in phase 2 clinical trials for AD,[31] but their mechanisms of action are unknown. In analogy to full-length Aβ, the high cytotoxicity observed for Aβ(25–35) is mediated through oligomers associated with self-assembly into amyloid fibrils.[52,53] Significantly, Aβ(25–35) induces a similar pattern of neural injury in organotypical hippocampal slices to that of Aβ42[54] and single chain variable domain antibody fragments against Aβ(25–35) prevent fibril formation and attenuate toxicity of $A\beta_{42}$ in vitro.[55] Because of its limited size, Aβ(25–35) has been extensively studied by computational[56−59] and experimental[53] techniques. Furthermore, the effect of EGCG[60] on morphology and toxicity of Aβ(25–35) oligomers was characterized. This vast amount of data makes Aβ(25–35) an ideal model system to rigorously assess the capability of IMS–MS to directly reveal the morphologies of early, soluble peptide oligomers, to determine the structural implications of ligands on amyloid self-assembly and finally to correlate this structural information to published cytoprotective effects induced by these ligands.

RESULTS

β-Sheet Aβ(25–35) Oligomers Emerge at the Dimer, and the Transition from Isotropic to β-Sheet Oligomers Is Completed at the Aβ(25–35) Pentamer. The ESI-Q mass spectrum of Aβ(25–35) shows abundant formation of soluble, transient oligomers (Figure 1A). Peaks are annotated with their n/z ratio, where n is the oligomer number and z is the charge, indicating abundant formation of n/z = 1/2 (m/z = 530), n/z = 2/3 (m/z = 707) and n/z = 3/4 (m/z = 795) and n/z = 1/1 (m/z = 1060), whereas less abundant peaks are found at n/z = 3/5 (m/z = 638), n/z = 5/7 (m/z = 757), n/z = 7/9 (m/z = 824) and n/z = 4/5 (m/z = 848). The corresponding ESI-qTOF[61] spectrum (Supporting Information, Figure S1A) reveals formation of oligomers up to the dodecamer (n/z = 12/7; m/z = 1818) and the general level of background counts above m/z = 1500 suggests existence of larger peptide oligomers in the sample that the ESI-qTOF instrument is not able to resolve.

Mass-selected arrival time distributions (ATDs) allow determination of accurate collision cross sections (CCS) for these Aβ(25–35) oligomers and thus provide detailed structural information on the individual aggregation states (Figure 2A,B, Supporting Information, Figure S3 and Table S3). The ATDs typically display multiple features (Supporting Information, Figure S3), indicating the presence of several conformations of the same oligomers or distinct oligomers with different n/z but the same m/z. Figure 2B displays the development of measured CCSs for pure Aβ(25–35) oligomers as a function of oligomer size n up to the octamer, which was the largest unambiguously assigned Aβ(25–35) oligomer based

dx.doi.org/10.1021/ja406197f | J. Am. Chem. Soc. 2013, 135, 16926–16937

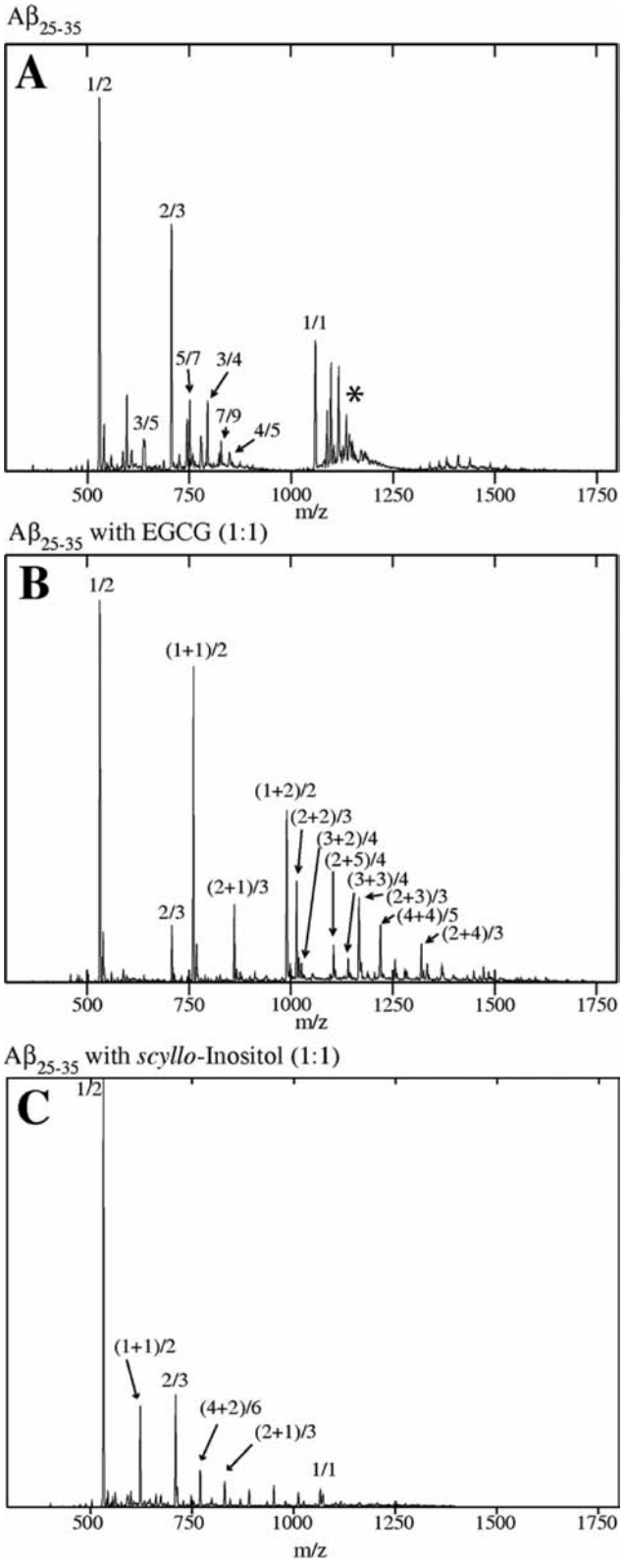

Figure 1. Mass spectra of Aβ(25−35) (A) and Aβ(25−35) incubated with EGCG at 1:1 (B) and Aβ(25−35) with *scyllo*-inositol at 1:1 (C) ratio. In all cases the Aβ(25−35) concentration was 200 μM in pure water solvent. Peaks are annotated by the oligomer size-to-charge (n/z) ratio. hetero-oligomers of Aβ(25−35) with ligands are labeled by ($n + m$)/z where m is the number of ligands. (see section S7 in the Supporting Information for a discussion of the peaks labeled by an asterisk).

on the m/z value. The experimental data are compared to three different structural models. First, the ideal isotropic growth model is included where oligomers grow equally in all spatial dimensions.[43] Here, the cross section σ grows as $n^{2/3}$ with increasing oligomer number n. The second limiting case is growth as an ideal in-register β-sheet (extracted from crystallographic data,[62] see Supporting Information section S3.1.1), where the cross section increases linearly with increasing oligomer number n.[43] Finally, oligomer growth as an ideal out-of-register β-sheet is included, where each monomer chain is shifted by one amino acid residue with respect to the neighboring one (labeled "triclinic" in Figure 2). These idealized oligomer growth modes offer limiting cases for the development of cross sections with increasing oligomer size n and thus guide the structural interpretation of the IMS−MS data. The data for the pure Aβ(25−35) system (Figure 2A, 2B, and Supporting Information, Figure S3 and Table S3) reveal oligomers consistent with isotropic topologies for the monomer through the tetramer. However, oligomers larger than the tetramer are inconsistent with isotropic structures, and instead correlate with extended, β-sheet geometries. These extended oligomer conformations emerge at the dimer, and increase in significance for the trimer and tetramer species until they predominate for the pentamer and larger oligomers (Figure 2B). Specifically, two distinct n/z = 2/3 dimer species are observed in the m/z = 707 ATD of pure Aβ(25−35) (Figure 2A), where the isotropic dimer conformation (395 Å^2) strongly prevails in abundance over the extended dimer (413 Å^2). A variety of intermediate oligomer species with CCSs larger than expected for isotropic, but smaller than expected for β-sheet topologies coexist for the trimer and tetramer (Figure 2B). These intermediate trimer and tetramer conformations suggest that the conformational transition from a prevailing isotropic dimer into a predominantly β-sheet tetramer topology occurs via a complex steady-state of different trimers and tetramers.

This conformational transition from prevalent isotropic dimer to β-sheet tetramer is the pivotal process for formation of amyloid fibrils of Aβ(25−35) from a presumed monomeric peptide chain. The IMS−MS data reveal that this structural conversion of Aβ(25−35) oligomers proceeds via a complex steady-state of intermediate trimer and tetramer conformations. In order to gain insight into the possible molecular topologies of these intermediate oligomeric species, the IMS−MS data were compared to recently published temperature replica-exchange molecular dynamics (T-REMD) simulations (see Supporting Information, section S1.2.5 for details).[59] The simulations indicate that the monomer takes on a folded, compact conformation dominated by a central turn motif (Supporting Information, Table S2). Compact, β-turn/coil and β-hairpin conformations (266 Å^2 and 267 Å^2) dominate the simulations and are in reasonable agreement with the experimental cross section (248 Å^2). The simulations further reveal a number of stable dimers, including coiled and β-sheet conformations. Predicted CCSs range from 411 Å^2 for the most compact, folded dimer to 464 Å^2 for the strongly extended β-sheet dimer. Comparison with the experiment reveals that compact Aβ(25−35) dimers prevail in the experiment (392 Å^2). Slightly extended dimers (413 Å^2) are experimentally observed, but fully extended β-sheet dimers are not. This discrepancy between experiment and theory can be rationalized by assuming that either Aβ(25−35) dimers are able to (partially) fold into gas-phase conformations during the time-scale of the experiment or that the extended β-sheet dimer

dx.doi.org/10.1021/ja406197f | J. Am. Chem. Soc. 2013, 135, 16926−16937

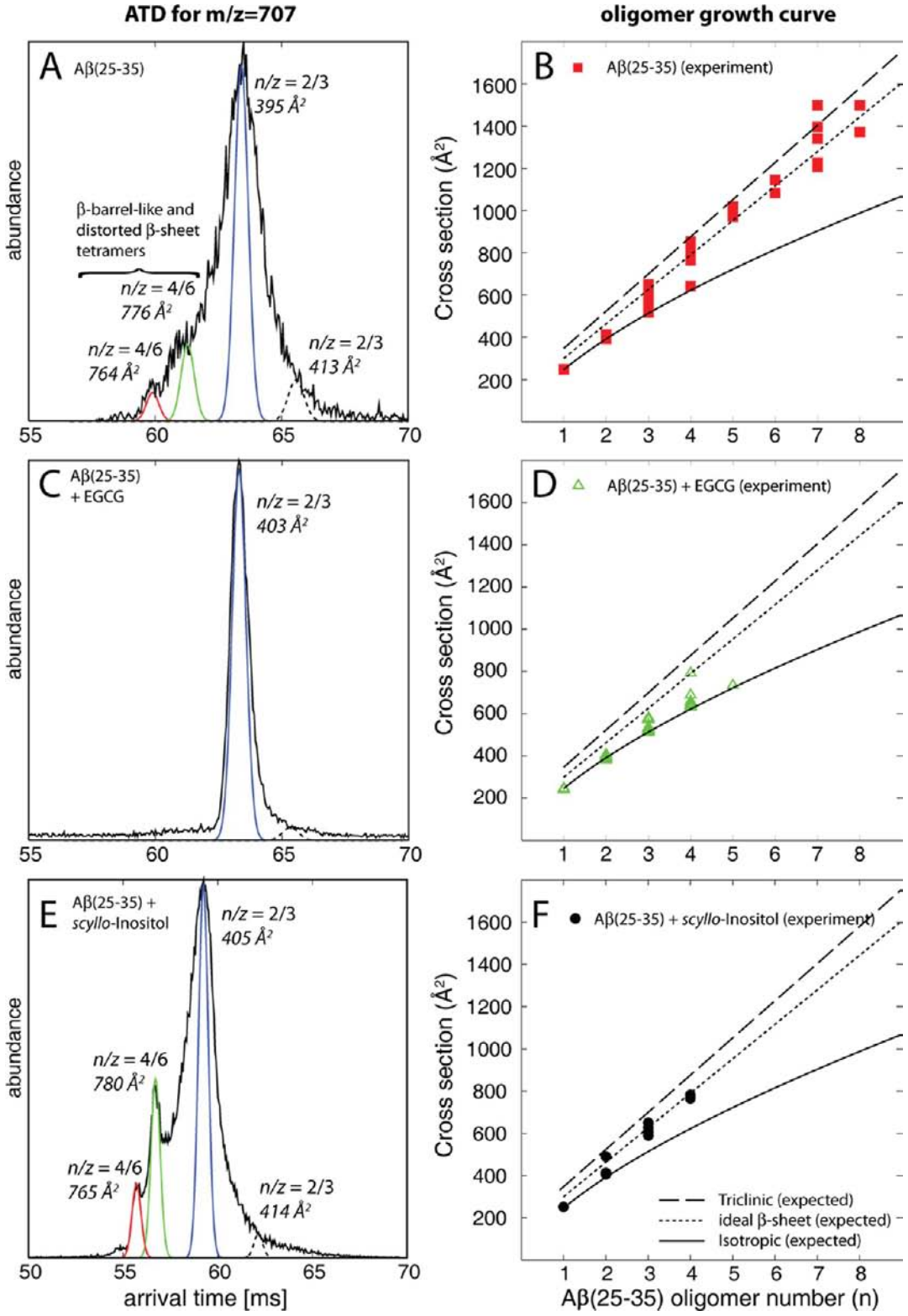

Figure 2. Ion mobility data of Aβ(25−35) (A, B), Aβ(25−35) with EGCG (C),(D) and Aβ(25−35) with *scyllo*-inositol (E, F). The Aβ(25−35):ligand ratios were 1:1 for both ligands. The lines in panels B, D, and F are defined in panel F (see text).

population is too small to be detected (predicted at 2.3% by theory). Extended-coil and extended−β conformations (580 and 610 Å^2) take on increased significance for the Aβ(25−35) trimer and coiled, highly compact trimer species are not observed in the simulations. The predicted CCSs for these conformations agree well with the experimental CCSs (557 to 650 Å^2), except for the largest experimentally observed peak. Since the T-REMD simulation samples the conformational distribution of a specific oligomer at thermal equilibrium, the relative populations of each conformation can be shifted with respect to the experiment where the steady-state system among various oligomer sizes is probed. The kinetic factor of the

dx.doi.org/10.1021/ja406197f | J. Am. Chem. Soc. 2013, 135, 16926−16937

aggregation cascade, which is not captured in T-REMD simulations, can favor the sampling of aggregation-prone conformations in the experiment that are predicted less stable and less abundant according to the simulation. Extended conformations continue to increase in abundance for the Aβ(25−35) tetramer (CCSs range from 707 Å^2 to 776 Å^2), and the simulations indicate the emergence of β-barrel tetramer conformations (716 Å^2). Again, the predicted CCSs agree well with the experimental results except for the largest species experimentally observed as noted for the trimer.

The strong correlation between the measured cross sections and those computed for the model structures of Aβ(25−35) oligomers thus support the view that the distinct Aβ(25−35) dimers, trimers and tetramers observed in the experiment differ from each other in the β-strand content of the individual Aβ(25−35) chains and that the prevalence of β-sheet character increases from dimers to tetramers.

Summarizing, the overall self-assembly of Aβ(25−35) as revealed by IMS−MS involves isotropic conformations up to the tetramer but as early as the dimer an intermediate aggregation stage begins in which a structural conversion between isotropic and β-sheet dominated conformations take place. The conformational transition is completed at the Aβ(25−35) pentamer and self-assembly continues as growth of β-sheet assemblies. The prevalence of β-sheet conformation suggested by the IMS−MS data is supported by the circular dichroism (CD) spectra (see Supporting Information, Figures S6, S7) and the observation of fibrillar aggregates by atomic force microscopy (AFM), Figure 3A and Supporting Information, Figures S9, S10) for aliquots taken from the same Aβ(25−35) sample that was used for IMS−MS analysis.

Epigallocatechin Gallate (EGCG) Competitively Binds to Aβ(25−35) Oligomers, Induces Isotropic Conformations and Prevents the Conversion from Isotropic to β-Sheet Aβ(25−35) Oligomers. The steady-state oligomer distribution of Aβ(25−35) is significantly altered by incubation with EGCG. First, the only Aβ(25−35) homooligomers identified in the presence of EGCG are Aβ(25−35) monomers and dimers (m/z = 530 and m/z = 707, Figure 1B and Supporting Information, Figure S2). The remaining peaks are identified as Aβ(25−35):EGCG hetero-oligomers. Second, only one oligomer with more than four Aβ(25−35) chains was found in the presence of EGCG (n/z = (5 + 3)/5; Supporting Information, Figure S4), which was of low abundance. Finally, isotropic topologies are found to strongly predominate the oligomer steady-state in the presence of EGCG, and the only oligomer observed to take on an extended conformation is the n/z = (4 + 4)/5 species (Supporting Information, Figure S4).

The predominance of isotropic Aβ(25−35) oligomer conformations in the presence of EGCG is further highlighted when correlating the CCSs of Aβ(25−35):EGCG hetero-oligomers with the number of EGCG molecules contained within the supermolecule (Figure 4). The cross sections extrapolated to free Aβ(25−35) monomers (σ_{extr} = 253 Å^2), dimers (σ_{extr} = 409 Å^2), trimers (σ_{extr} = 560 Å^2) and tetramers (σ_{extr} = 653 Å^2) agree strongly with those of the compact, isotropic oligomers observed in the steady-state of pure Aβ(25−35) ($\sigma_{isotropic}$ = 249 Å^2 (monomer), 395 Å^2 (dimer), 518 Å^2 (trimer) and 627 Å^2 (tetramer), respectively). Oligomers that are centrally implicated in the conformational transition from isotropic to β-sheet conformations of pure Aβ(25−35) are absent in the presence of EGCG. One example is the absence of the two extended n/z = 4/6 Aβ(25−35) homotetramers with substantial β-strand character in the m/z = 707 peak (c.f. Figure 2A,C). Additionally, the cross section data

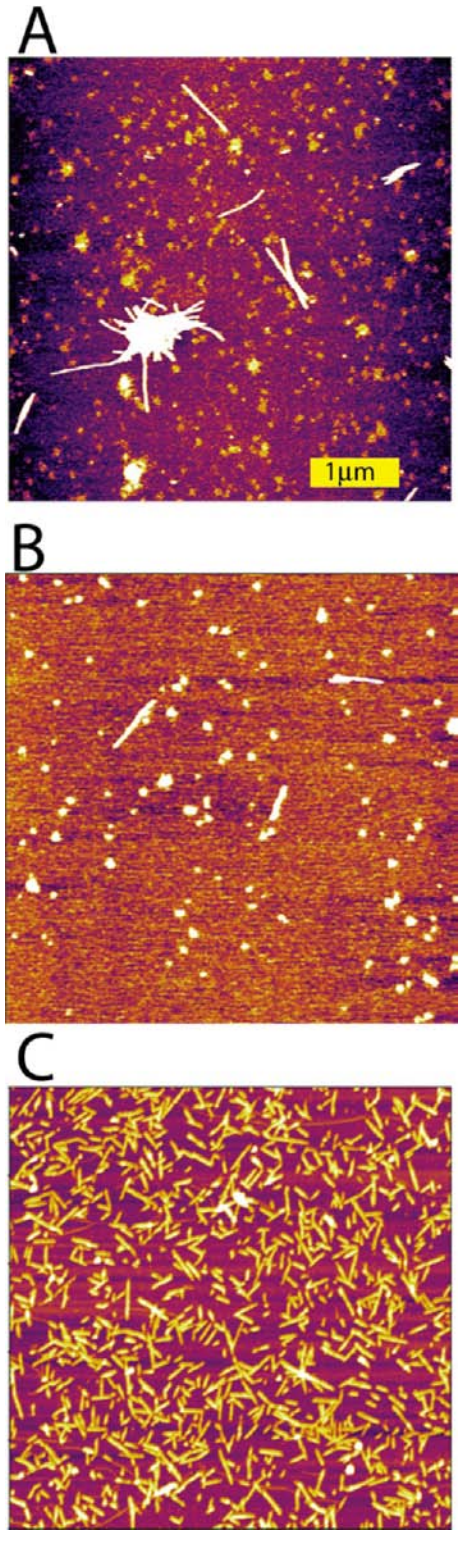

Figure 3. AFM images of Aβ(25−35) (A), and Aβ(25−35) with EGCG at 1:1 (B) and Aβ(25−35) with *scyllo*-inositol at 1:1 (C) ratios. (A) Abundant Aβ(25−35) fibrils with an average diameter of 1 μm are visible in the absence of EGCG and *scyllo*-inositol. (B) Fibril formation is impeded by EGCG, and granular aggregates are observed. (C) *Scyllo*-inositol redirects Aβ(25−35) assembly into smaller, fibrillar macroscopic aggregates.

dx.doi.org/10.1021/ja406197f | J. Am. Chem. Soc. 2013, 135, 16926−16937

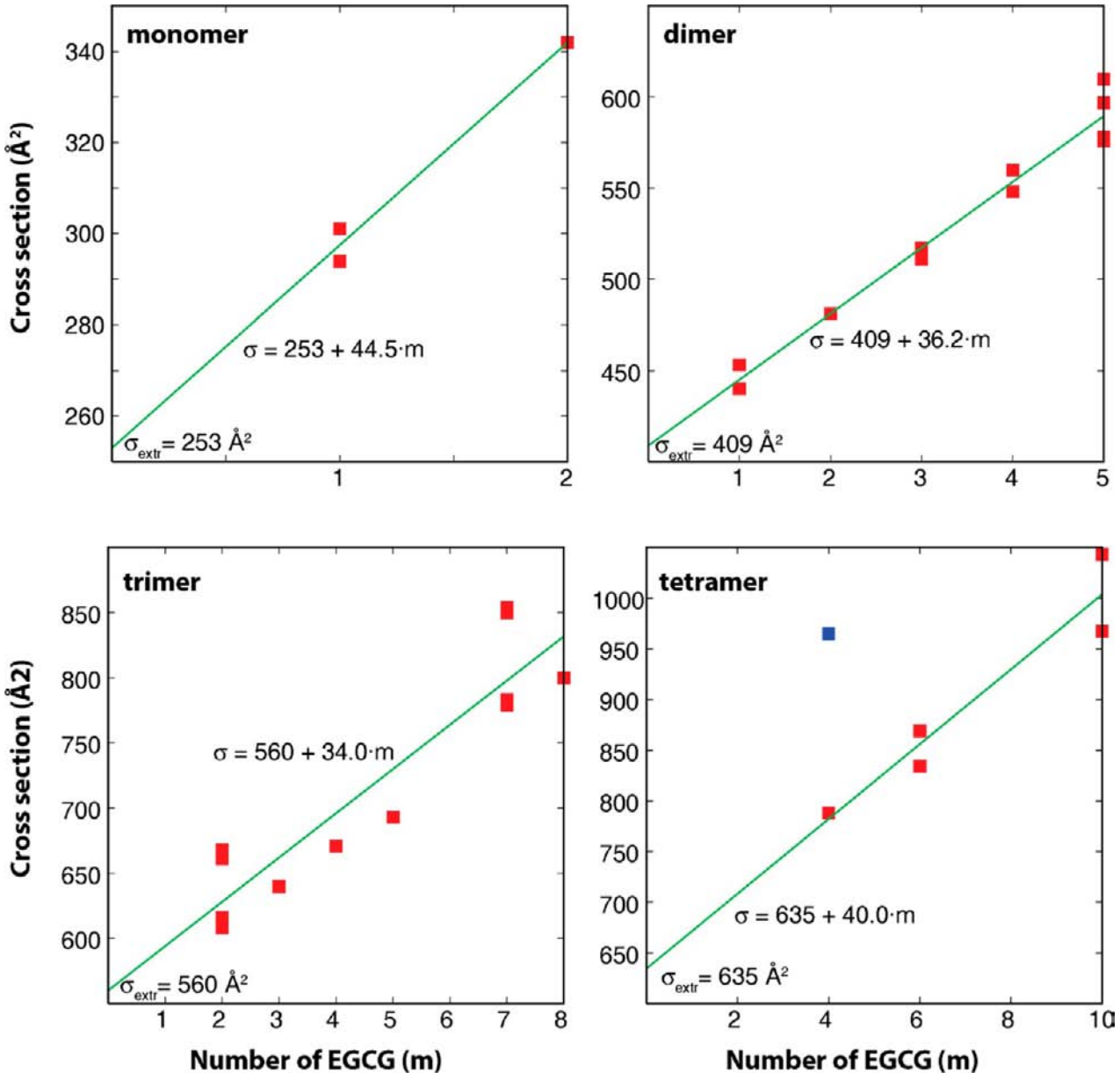

Figure 4. Extrapolation of cross sections of Aβ(25−35) oligomers (monomer, dimer, trimer, tetramer) complexed with EGCG to free Aβ(25−35).

indicate an isotropic conformation for the only observed pentamer (n/z = (5 + 3)/5, m/z = 1336), demonstrating that the conformational transition to β-sheet Aβ(25−35) oligomers does not occur in the presence of EGCG. These observations underscore that oligomers with β-strand character of Aβ(25−35) chains are suppressed by the presence of EGCG. Thus, the IMS−MS data reveals that EGCG competitively suppresses the formation of Aβ(25−35) homooligomers and instead induces isotropic conformations by formation of Aβ(25−35):EGCG hetero-oligomers. CD data (Supporting Information, Figure S6, S7) support the absence of β-sheet Aβ(25−35) oligomer conformations in the presence of EGCG. Additionally, EGCG is found to complex Aβ(25−35) oligomers and to suppress formation of Aβ(25−35) fibrils in a concentration-dependent manner (Supporting Information, Figure S1, S9). Furthermore, AFM imaging reveals that EGCG partially remodels matured Aβ(25−35) fibrils into granular aggregates (see Supporting Information, Figure S10). These observations suggest that EGCG is able to induce isotropic conformations by binding strongly to soluble Aβ(25−35) oligomers. Previous studies[25,28,29,31,63] showed a similar effect of EGCG on morphology and toxicity of several amyloid forming peptides, including α-synuclein and Aβ_{42}.

Explicit solvent molecular dynamics (MD) simulations were carried out in order to elucidate the molecular mode of how EGCG induces isotropic Aβ(25−35) oligomer conformations. To this end, the aggregation of four Aβ(25−35) peptides were simulated in the absence and the presence of four EGCG molecules (see Supporting Information, section S1.2.4 for details). Interacting pairs of Aβ(25−35)/Aβ(25−35) and EGCG/Aβ(25−35) were identified during the simulations at regular time-intervals independent of the particular oligomeric state. Subsequently, the secondary structure of the Aβ(25−35) chain was characterized by means of the phi/psi angles of the amide bonds as α-helix, β-sheet, or coil conformation. Figure 5A depicts the secondary structure propensities for Aβ(25−35) chains observed in the absence and in the presence of EGCG. Figure 5A reveals that ordered (i.e., β-strand and helical)

dx.doi.org/10.1021/ja406197f | J. Am. Chem. Soc. 2013, 135, 16926−16937

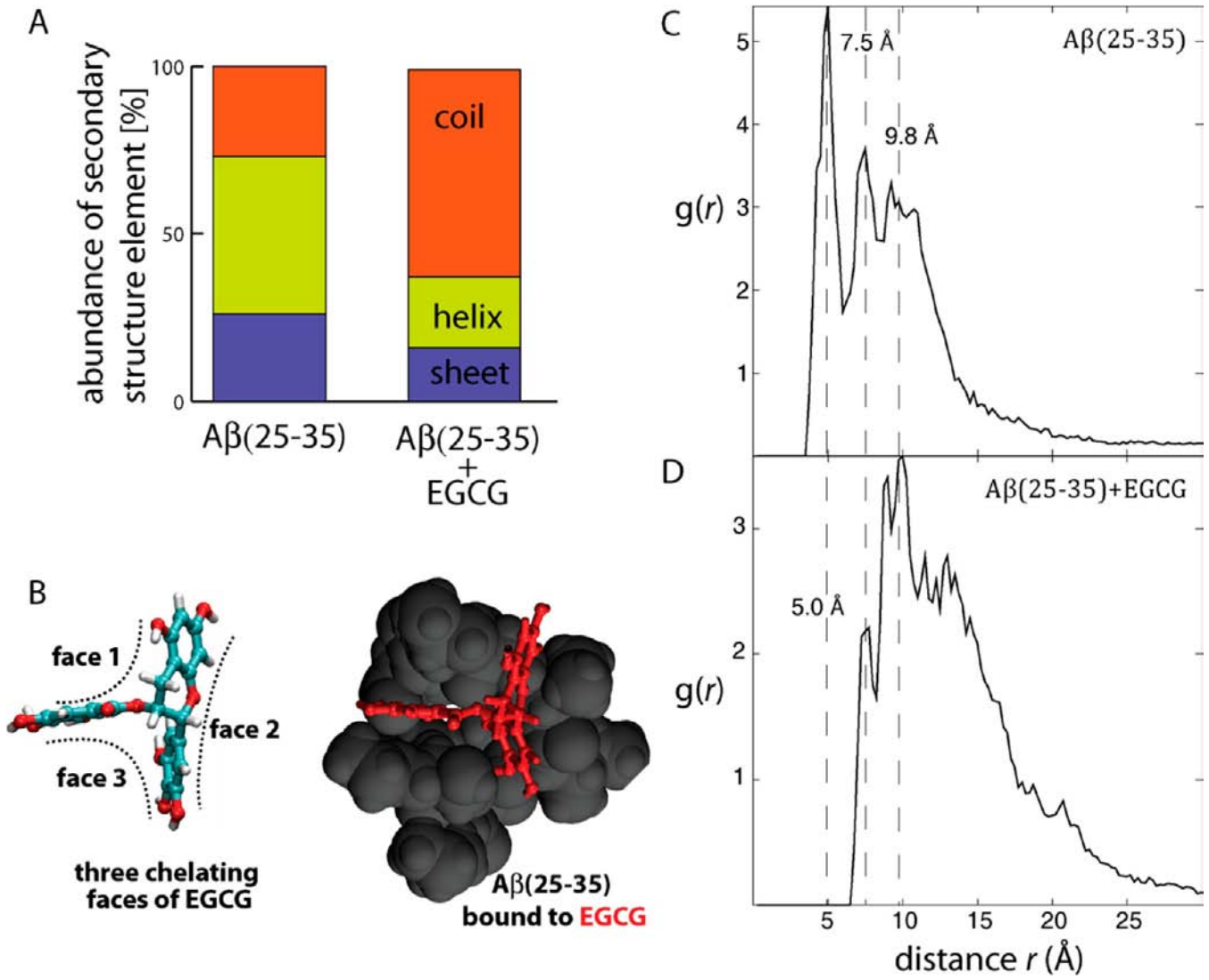

Figure 5. Results obtained by explicit solvent molecular dynamics simulations of Aβ(25−35) and EGCG. (A) Secondary structure propensities observed for Aβ(25−35) chains in the absence and presence of EGCG. (B) Representative structures for the pairwise interactions present in pure Aβ(25−35) (left) and EGCG:Aβ(25−35) (right). (C, D) Radial distribution functions (RDFs) g(r) of Aβ(25−35) chains in the absence and presence of EGCG. The RDF g(r) is compiled using the center-of-mass distances r for each combination of pairs of Aβ(25−35) chains at each snapshot from the MD simulation. The presence of EGCG increases the most likely distance of two Aβ(25−35) chains from approximately 5.0 Å to 9.8 Å.

conformations of Aβ(25−35) chains predominate in the absence of EGCG. The Figure further shows that binding to EGCG increases prevalence of unordered Aβ(25−35) coil conformations from approximately 27 to 62% and reduces the ordered conformations (β-strand and helical) from approximately 73 to 37%, respectively. These observations are consistent with the experimental IMS−MS data in the sense that the presence of EGCG favors isotropic Aβ(25−35) oligomer conformations over ordered, β-strand conformation of Aβ(25−35) oligomers. Why and how, at a molecular level, does EGCG induce unstructured, coiled Aβ(25−35) conformations? To investigate this question, the geometries of Aβ(25−35) chains that are bound to EGCG were extracted from the simulation and the surface area by which Aβ(25−35) and EGCG bind to each other was determined for each such complex. The details of the corresponding analysis can be found in the Supporting Information, Figure S11, but the key finding is as follows. The geometry of EGCG can be viewed as a collection of three distinct aromatic rings arranged in a rigid, propeller-like geometry (Figure 5B). As a consequence of this geometry, EGCG has three faces through which it can bind to hydrophobic (aromatic rings) and hydrophilic (hydroxyl groups) patches on Aβ(25−35). Each such face can be individually bound to Aβ(25−35) but EGCG becomes increasingly stronger bound by successively binding to the peptide with two and three faces (see Supporting Information, Figure S11). However, the tridentate binding mode of EGCG can only be accomplished if the bound Aβ(25−35) chain takes on a globular, unordered structure, but cannot be accomplished with the peptide adopting an ordered, helical or β-strand conformation. For this reason, EGCG effectively prevents the formation of oligomeric species that have the correct geometry to further self-assemble into amyloid fibrils.

Pair-wise radial distribution functions $g(r)$ (RDFs) were compiled from the simulation data in the absence and presence of EGCG (Figure 5C,D). The RDFs were compiled from all

dx.doi.org/10.1021/ja406197f | J. Am. Chem. Soc. 2013, 135, 16926−16937

pairwise center-of mass-distances r for each snapshot sampled during the simulations. RDFs allow the determination of coordination shells and thus reveal differences in binding modes of Aβ(25−35) peptides in the absence and presence of EGCG. The analysis thus reveals how the binding of EGCG to a Aβ(25−35) chain affects the self-assembly process of Aβ(25−35). The first and second coordination shells in the absence of EGCG are found at 5.0 and 7.5 Å center-of-mass distance, respectively (Figure 5C), indicating a clear short-range order of Aβ(25−35) chains in the absence of EGCG. In particular, the first coordination sphere (5.0 Å) is in the order of the distance of an intermolecular hydrogen-bond and thus suggests a strong intermolecular alignment of Aβ(25−35) peptides in the absence of EGCG. It is further of note that this 5.0 Å intermolecular distance is similar to the 4.8 Å that is typically found in amyloid fibers. However, in the presence of EGCG, this 5.0 Å coordination shell between two Aβ(25−35) chains is absent (Figure 5D). Instead, the first coordination shell of Aβ(25−35) chains in the presence of EGCG is observed at 7.5 Å center-of-mass distance, which was the second coordination shell of the pure Aβ(25−35) system. Further, the most likely coordination between two Aβ(25−35) chains in the presence of EGCG takes place at approximately 9.8 Å center-of-mass distance between two individual Aβ(25−35) chains. In sum, the simulation data show that EGCG increases the distance between two Aβ(25−35) peptides and eliminates strongly aligned, hydrogen-bonded Aβ(25−35) chains. Consequently, we conclude that EGCG inserts between two Aβ(25−35) peptides and disrupts their intermolecular binding, preventing the alignment of Aβ(25−35) peptides that is necessary for them to form stable β-sheet fibrillar oligomers.

In sum, the combined experimental and computational data presented here indicate that EGCG prevents the conformational transition from isotropic to barrel-like and β-sheet oligomers that was observed by IMS−MS to occur at the trimer and tetramer of pure Aβ(25−35). Significantly, the IMS−MS data indicate that EGCG competitively binds to small Aβ(25−35) species that occur on the self-assembly process earlier than the conformational transition observed for free Aβ(25−35), and EGCG thus prevents the conformational transition to β-sheet oligomers of Aβ(25−35) by preventing the formation of Aβ(25−35) homotrimers and −tetramers. As a consequence, formation of the barrel-like and β-sheet n/z = 4/6 tetramers is completely suppressed in the presence of EGCG (Figure 2C) and the formation of macroscopic fibrillar Aβ(25−35) aggregates is prevented (Figure 3B). Furthermore, the combined computational, AFM, CD and IMS−MS data presented here suggest that amyloid fibril remodeling by EGCG proceeds by extracting small oligomers from the macroscopic fibrillar aggregates by disrupting binding between two Aβ(25−35) entities and subsequently by invoking isotropic conformations in these smaller amyloid oligomers via complexation of the soluble Aβ(25−35) oligomers by EGCG. Another possible mode of fibril remodeling by EGCG is that EGCG shifts the steady-state oligomer distribution toward small, soluble non-β-sheet oligomers, effectively dissolving the macroscopic fibril by removing soluble, β-sheet Aβ(25−35) oligomers from the steady-state with the macroscopic fibril via inducing an unstructured conformation into Aβ(25−35) peptides, i.e. by Le Chatelier's principle.

Scyllo-inositol Binds Weakly to Aβ(25−35) Oligomers and Does Not Adversely Affect the Conversion of Aβ(25−35) Oligomers from Isotropic into Fibrillar Conformations. Figure 1C displays the mass spectrum of Aβ(25−35) incubated with *scyllo*-inositol at a 1:1 ratio. It is noted that Aβ(25−35) homooligomers (such as n/z = 2/3 (m/z = 707), 3/4 (m/z = 795) and 4/6 (m/z = 707)) are more abundantly formed than Aβ(25−35):*scyllo*-inositol hetero-oligomers (such as $(n + m)/z = (1 + 1)/2$; (m/z = 620) and $(n + m)/z = ((2 + 1)/2$; (m/z = 710)). Furthermore, the cross section data (Figure 2E,F and Supporting Information, Figure S5) indicate that extended Aβ(25−35) homooligomers are slightly increased in abundance when compared to the pure Aβ(25−35) sample. One example of enhanced population of extended species are the n/z = 4/6 tetramers in the m/z = 707 ATD (Figure 2E). These observations indicate that *scyllo*-inositol binds relatively weakly to Aβ(25−35) and its oligomers and thus may reduce the overall abundance of Aβ(25−35) homooligomers. However, strongly extended dimers (491 Å^2) are observed at m/z 530 (Supporting Information, Figure S5). These strongly extended dimers agree well with extended β-strand dimers observed in the simulations at low abundance (496 Å^2, Supporting Information, Table S2), but not found in pure Aβ(25−35) or when incubated with EGCG. Consequently, *scyllo*-inositol is found unable to prevent the transition of Aβ(25−35) homooligomers into β-sheet-like trimers and tetramers conformations (Figure 2F). In fact, the IMS−MS data indicate that the presence of the n/z = 4/6 tetramer conformations with intermediate cross sections (765 and 780 Å^2) are enhanced with respect to the pure Aβ(25−35) system (c.f. Figure 2A,E). These conclusions drawn from the IMS−MS data are supported by AFM imaging of aliquots taken from the same sample (Figure 3C) showing highly abundant formation of fibrillar Aβ(25−35) aggregates, which is consistent with recently reported abundant formation of fibrillar aggregates and Thioflavin-T fluorescence of Aβ_{1-42} when incubated with *scyllo*-inositol.[31]

DISCUSSION

Protein aggregation into amyloid fibrils is considered a pathogenic process.[1] The amyloid cascade hypothesis[11] suggests that this pathogenic effect arises from cytotoxic protein oligomers that are transient components of an oligomer steady-state between the monomer and the mature, fibrillar aggregate. One fundamental problem of research related to amyloid formation and disease is that the specific structures and abundances of these oligomers are not amenable by bulk measurement techniques[64−69] which convolute the steady-state into one single entity. In particular, conformational transitions of transient, intermediate oligomers are not directly accessible by bulk measurements of the macroscopic aggregates. Therefore, structural properties of soluble oligomers during amyloid formation could not[9] or only vaguely[15] be linked to their toxicity, and, consequently, an *Ansatz* that guides the rational development of therapeutic strategies to amyloid diseases does not exist to date.[70] Recent failures of a number of clinical trials[71] emphasize the challenge of traditional bulk techniques to relate structural information with cytotoxic activity and underline the urgency to develop a deeper understanding of the molecular mechanisms that are directly responsible for amyloid diseases.

In the current work, IMS−MS is used to unveil the structural polymorphism of Aβ(25−35) oligomers and to reveal the effect of two assembly modulators currently in clinical trials for AD[16] on Aβ(25−35) self-assembly. The data show that the self-assembly of Aβ(25−35) in the absence of assembly modulators

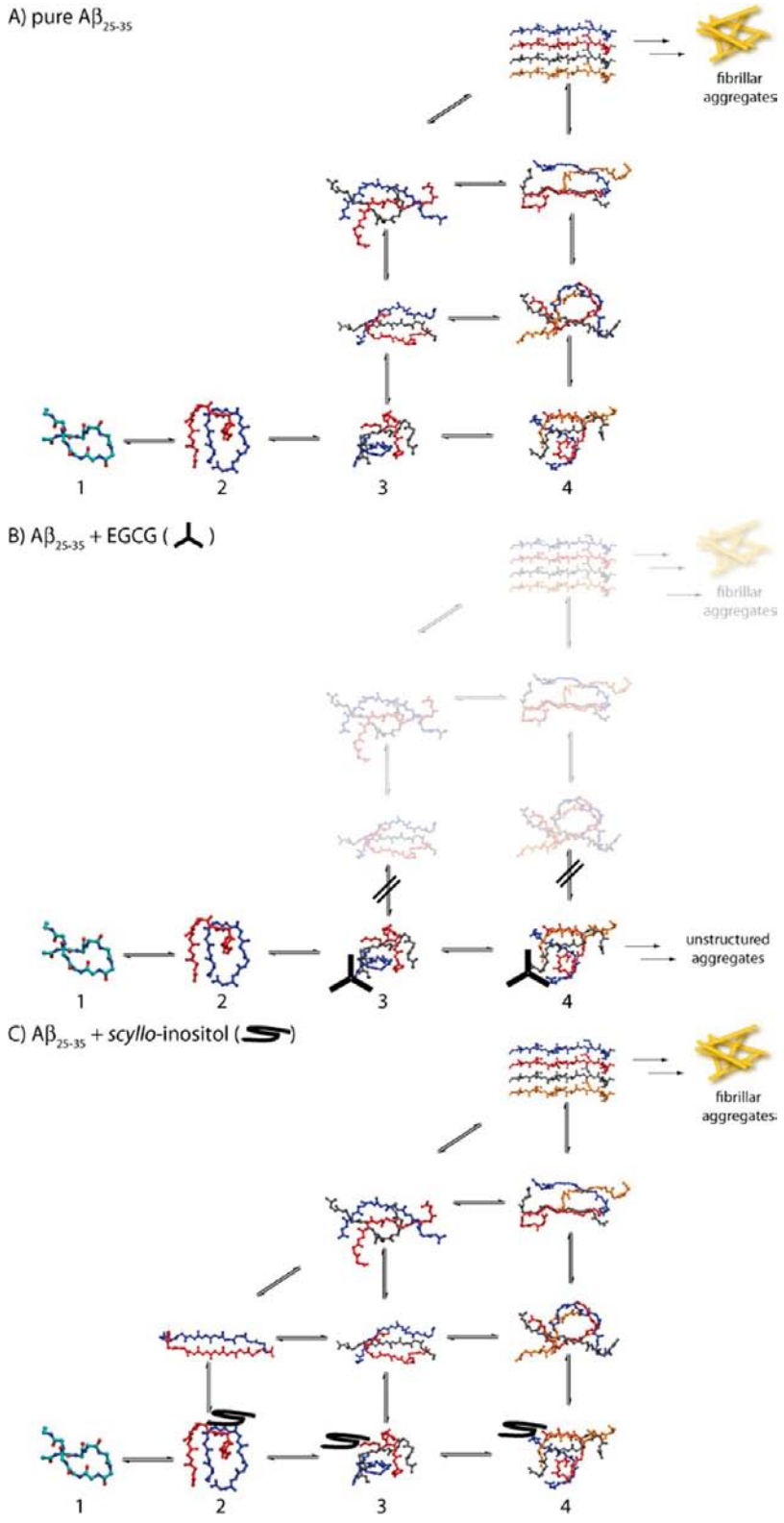

Figure 6. Proposed assembly pathways of Aβ(25−35) in absence (A) and presence of EGCG (B) and *scyllo*-inositol (C). (A) The self-assembly pathway of Aβ(25−35) is proposed to proceed from compact, coiled monomers and dimers into β-extended larger oligomers via a conversion from coiled to β-extended conformations at the trimer and tetramer. A number of different oligomer conformations are identified in the IMS−MS data for the trimer and tetramers including (distorted) β-sheet and β-barrel-like species. (B) EGCG strongly binds to the earliest Aβ(25−35) oligomers before the onset of the conformational transition and induces isotropic geometries of Aβ(25−35):EGCG hetero-oligomers. Thus, fibrillar and β-barrel-like oligomeric species are not present in the presence of EGCG. (C) *Scyllo*-inositol binds only weakly to Aβ(25−35) oligomers, and does not induce isotropic oligomer structures. Thus, (distorted) β-sheet and β-barrel-like Aβ(25−35) homooligomers are observed in the presence of *scyllo*-inositol.

dx.doi.org/10.1021/ja406197f | *J. Am. Chem. Soc.* 2013, 135, 16926−16937

(Figure 6A) proceeds from compact, coiled monomers and dimers into β-extended oligomers with a marked conversion from coiled to β-extended conformations at the trimer and tetramer. A plethora of different oligomer conformations can be identified by the IMS−MS data for the trimer and tetramers including distorted β-sheet and β-barrel-like species. Such β-oligomers can potentially insert into cellular membranes and thus impair membrane stability and may consequently attenuate cell viability.[72] *Scyllo*-inositol is found to bind to Aβ(25−35) oligomers, in accord with recent computational results.[73] Therefore, *scyllo*-inositol can potentially influence the assembly of Aβ(25−35) oligomers. However, the IMS−MS data reveal that *scyllo*-inositol binds only weakly (Figure 1C) and does not significantly affect the conformational transition of Aβ(25−35) homooligomers (Figure 2E,F) at the concentrations used in this work. Importantly, population of the β-barrel-like and β-sheet n/z = 4/6 tetramer species appears enhanced, and a strongly extended dimer species emerges in the presence of *scyllo*-inositol when compared to the pure Aβ(25−35) system (Figure 2E,F and Supporting Information, Figure S5). Consequently, fibrillar aggregates are found by AFM imaging in the presence of *scyllo*-inositol (Figure 3C). These findings are in accord with a recent study[31] that reported strong Thioflavin T fluorescence and complete lack of cytoprotective effects when Aβ_{1-42} was incubated at even higher *scyllo*-inositol:peptide ratios than used in the current work. However, other prior studies reported therapeutic effects at much higher concentrations.[32] Thus, the IMS−MS data presented in this work suggest that *scyllo*-inositol reduces the effective amyloid peptide concentration by binding weakly to oligomers, and thus may indirectly attenuate oligomer toxicity at elevated concentrations. However, the data obtained in this work demonstrate that *scyllo*-inositol does not directly modulate the pathogenic agents that are transiently populated during amyloid formation.

In contrast to *scyllo*-inositol, EGCG is shown to bind strongly to Aβ(25−35) oligomers and to effectively attenuate formation of larger Aβ(25−35) homooligomers. Furthermore, EGCG is able to induce isotropic conformations in EGCG:Aβ(25−35) hetero-oligomers and thus clearly prevents the transition of Aβ(25−35) homooligomers into β-extended structures at the trimer and tetramer. Significantly, EGCG completely suppresses formation of the β-barrel-like and β-sheet n/z = 4/6 tetramers. These observations confirm previous suggestions of the molecular mode of action of EGCG that were made based on studies on the interaction of EGCG with full-length Aβ_{42}[63] and α-synuclein[28,29] that implied EGCG induces unstructured oligomers by interfering with an early event in amyloid formation. The current results suggest that the rather rigid molecular geometry of EGCG and its ability to provide three chelating faces to bind Aβ(25−35) is key to the prevention of Aβ(25−35) β-strand oligomers. It is furthermore significant that the IMS−MS data indicate that EGCG interferes with the Aβ(25−35) self-assembly cascade and induces isotropic conformations *before the onset of the structural transition from random to β-assembly*.

CONCLUSIONS

Here we use IMS−MS, molecular dynamics modeling and AFM to study the oligomerization of the important amyloid β-protein fragment Aβ(25−35) and to observe the effect of two amyloid inhibitors currently in clinical trials on the oligomerization/amyloid formation of the peptide. Our findings include the following:

- IMS−MS data indicate Aβ(25−35) initiates oligomerization isotropically, undergoes a transition to β-sheet structures from n = 3 to n = 4 and above n = 4 forms only β-sheet oligomeric structures. Oligomer distributions and structures were independent of Aβ(25−35) concentration in the range from 25 to 250 μM indicating solution processes were being observed.
- The addition of EGCG yields mixed Aβ(25−35)/EGCG oligomers with up to three EGCG ligands attached per Aβ(25−35) peptide. No β-sheet oligomers are observed in these mixtures at any value of n even for nonligated Aβ(25−35). The addition of EGCG serves to divert Aβ(25−35) oligomers to compact, near isotropic structures.
- The addition of *scyllo*-inositol reduces the extent of oligomer formation in Aβ(25−35) but does not remove β-sheet structures in the oligomers, and thus is ineffective as an inhibitor at the concentrations used here.
- AFM measurements on the above listed sample solutions indicate fibril formation in pure Aβ(25−35), no fibrils and only granular aggregates when EGCG is added, and smaller but still fibrillar structures when *scyllo*-inositol is added. The completely complementary nature of these results to the IMS−MS results provides support that IMS−MS reports actual solution oligomer distributions and structures.
- MD studies indicate that EGCG interacts with Aβ(25−35) through its three planar ring system, resulting in folds in the peptide that eliminate the possibility of β-structure formation. It is reasonable to suggest this mechanism is responsible for the fact that EGCG is a broad spectrum amyloid inhibitor.

METHODS

A full description of methods is given in Supporting Information. Briefly, for IMS−MS samples were dissolved in water to the desired concentration, loaded into gold coated nanoESI capillaries, and electrosprayed on home-built instruments.[74] Ions are focused, stored in an ion funnel, and pulsed into a drift tube filled with 13 Torr of He. They are pulled through the drift tube under the influence of a weak electric field. At the end of the drift tube ions of a particular oligomeric state are mass selected and their arrival time distribution (ATD) is recorded. The arrival time is related to the collision cross-section of the ion (see Supporting Information). Molecular dynamics calculations were carried out with the Amber simulation package[75] in conjunction with the ff03 force field.[76,77] Theoretical cross sections were computed by the trajectory[78] and PSA methods.[79−81] For AFM images aliquots of the same peptide sample solutions were drop cast onto freshly cleaved mica slides and imaged on a MFP-3D-SA instrument (AsylumResearch, Santa Barbara). CD spectra were recorded on OLIS (Instrument, Inc.) DSM 1000 RSM and AVIV (Biomedical Inc.) circular dichroism spectrophotometers.

ASSOCIATED CONTENT

Supporting Information

Full description of materials and sample preparation, ion mobility spectrometry, circular dichroism (CD), atomic force microscopy (AFM), molecular dynamics (MD), and cross section calculations. Mass spectra, arrival time distributions (ATDs), CD spectra, and AFM images of pure amyloid-β(25−35) and in the presence of epigallocatechin-gallate (EGCG)

and *scyllo*-inositol, respectively. This information is available free of charge via the Internet at http://pubs.acs.org.

AUTHOR INFORMATION

Corresponding Author

bowers@chem.ucsb.edu

Author Contributions

†C.B. and T.D.D. contributed equally.

Notes

The authors declare no competing financial interest.

ACKNOWLEDGMENTS

We thank Dr. Luca Larini for providing the solvent-free Aβ(25-35) simulations. This research was supported by the National Science Foundation under Grant CHE-0909743 (MTB). A prototype Synapt instrument was graciously provided by the Waters Corporation. C.B. is grateful to the Alexander-von-Humboldt-Foundation for a Feodor-Lynen-Fellowship. N.J.E. acknowledges the National Science Foundation Graduate Student Research Fellowship. S.K.B. acknowledges funding from the MURI and DURIP programs of the U.S. Army Research Laboratory and U.S. Army Research Office under Grant Nos. DAAD 19-03-1-0121 and W911NF-09-1-0280 for purchase the AFM instrument. Support from the National Science Foundation (MCB-1158577) and the David and Lucile Packard Foundation are gratefully acknowledged. This work used the Extreme Science and Engineering Discovery Environment (XSEDE), which is supported by National Science Foundation Grant No. OCI-1053575. The authors acknowledge the Texas Advanced Computing Center (TACC) at The University of Texas at Austin and the National Institute for Computational Sciences at Oak Ridge National Laboratory for providing HPC resources through the XSEDE Grant No. TG-MCA05S027. We acknowledge support from the Center for Scientific Computing at the CNSI and MRL: an NSF MRSEC (DMR-1121053) and NSF CNS-0960316.

REFERENCES

(1) Chiti, F.; Dobson, C. M. *Nat. Chem. Biol.* **2008**, *5*, 15−21.
(2) Finder, V. H. *J. Alzheimers Dis.* **2010**, *22*, S5−S19.
(3) Ross, C. A.; Poirier, M. A. *Nat. Rev. Mol. Cell Biol.* **2005**, *6*, 891−898.
(4) Kayed, R.; Head, E.; Thompson, J. L.; McIntire, T. M.; Milton, S. C.; Cotman, C. W.; Glabe, C. G. *Science* **2003**, *300*, 486−489.
(5) Bucciantini, M.; Giannoni, E.; Chiti, F.; Baroni, F.; Formigli, L.; Zurdo, J. S.; Taddei, N.; Ramponi, G.; Dobson, C. M.; Stefani, M. *Nature* **2002**, *416*, 507−511.
(6) Baglioni, S.; Casamenti, F.; Bucciantini, M.; Luheshi, L. M.; Taddei, N.; Chiti, F.; Dobson, C. M.; Stefani, M. *J. Neurosci.* **2006**, *26*, 8160−8167.
(7) Krafft, G. A.; Klein, W. L. *Neuropharmacology* **2010**, *59*, 230e242.
(8) Lambert, M. P.; Barlow, A. K.; Chromy, B. A.; Edwards, C.; Freed, R.; Liosatos, M.; Morgan, T. E.; Rozovsky, I.; Trommer, B.; Viola, K. L.; Wals, P.; Zhang, C.; Finch, C. E.; Krafft, G. A.; Klein, W. L. *Proc. Natl. Acad. Sci. U.S.A.* **1998**, *95*, 6448−6453.
(9) Bieschke, J.; Siegel, S. J.; Fu, Y.; Kelly, J. W. *Biochemistry* **2008**, *47*, 50−59.
(10) Bernstein, S. L.; Dupuis, N. F.; Lazo, N. D.; Wyttenbach, T.; Condron, M. M.; Bitan, G.; Teplow, D. B.; Shea, J.-E.; Ruotolo, B. T.; Robinson, C. V.; Bowers, M. T. *Nat. Chem.* **2009**, *1*, 326−331.
(11) Haass, C.; Selkoe, D. J. *Nat. Rev. Mol. Cell Biol.* **2007**, *8*, 101−112.
(12) Walsh, D. M.; Selkoe, D. J. *Protein Pept. Lett.* **2004**, *11*, 213−228.
(13) Hardy, J.; Selkoe, D. J. *Science* **2002**, *297*, 353−356.
(14) Mason, J. M.; Kokkoni, N.; Stott, K.; Doig, A. J. *Curr. Opin. Struct. Biol.* **2003**, *13*, 526−532.
(15) Bartolini, M.; Andrisano, V. *ChemBioChem* **2010**, *11*, 1018−1035.
(16) Liu, T.; Bitan, G. *ChemMedChem* **2012**, *0000*, 1−17.
(17) Bieschke, J.; Herbst, M.; Wiglenda, T.; Friedrich, R. P.; Boeddrich, A.; Schiele, F.; Kleckers, D.; Amo, J. M. L. d.; Grüning, B. A.; Wang, Q.; Schmidt, M. R.; Lurz, R.; Anwyl, R.; Schnoegl, S.; Fändrich, M.; Frank, R. F.; Reif, B.; Günther, S.; Walsh, D. M.; Wanker, E. E. *Nat. Chem. Biol.* **2012**, *8*, 93−101.
(18) Lambertoa, G. R.; Binolfia, A.; Orcelleta, M. L.; Bertoncinib, C. W.; Zweckstetter, M.; Griesingerc, C.; Fernandeza, C. O. *Proc. Natl. Acad. Sci. U.S.A.* **2009**, *106*, 21057−21062.
(19) Feng, B. Y.; Toyama, B. H.; Wille, H.; Colby, D. W.; Collins, S. R.; May, B. C. H.; Prusiner, S. B.; Weissman, J.; Shoichet, B. K. *Nat. Chem. Biol.* **2008**, *4*, 197−199.
(20) Zheng, X.; Gessel, M. M.; Wisniewski, M. L.; Viswanathan, K.; Wright, D. L.; Bahr, B. A.; Bowers, M. T. *J. Biol. Chem.* **2012**, *287*, 6084−6088.
(21) Gessel, M. M.; Wu, C.; Li, H.; Bitan, G.; Shea, J.-E.; Bowers, M. T. *Biochemistry* **2012**, *51*, 108−117.
(22) Bodner, R. A.; Outeiro, T. F.; Altmann, S.; Maxwell, M. M.; Cho, S. H.; Hyman, B. T.; McLean, P. J.; Young, A. B.; Housman, D. E.; Kazantsev, A. G. *Proc. Natl. Acad. Sci. U.S.A.* **2006**, *103*, 4246−4251.
(23) Sinha, S.; Lopes, D. H. J.; Du, Z.; Pang, E. S.; Shanmugam, A.; Lomakin, A.; Talbierskyz, P.; Tennstaedt, A.; McDaniel, K.; Bakshi, R.; Kuo, P.-Y.; Ehrmann, M.; Benedek, G. B.; Loo, J. A.; Klarner, F.-G.; Schrader, T.; Wang, C.; Bitan, G. *J. Am. Chem. Soc.* **2011**, *133*, 16958−16969.
(24) Ladiwala, A. R.; Lin, J. C.; Bale, S. S.; Marcelino-Cruz, A. M.; Bhattacharya, M.; Dordick, J. S.; Tessier, P. M. *J. Biol. Chem.* **2010**, *285*, 24228−24237.
(25) Huang, R.; Vivekanandan, S.; Brender, J. R.; Abe, Y.; Naito, A.; Ramamoorthy, A. *J. Mol. Biol.* **2012**, *416*, 108−120.
(26) Ferreira, N.; Cardoso, I.; Domingues, M. R.; Vitorino, R.; Bastos, M.; Bai, G.; Saraiva, M. J.; Almeida, M. R. *FEBs Lett.* **2009**, *583*, 3569−3576.
(27) Roberts, B. E.; Duennwald, M. L.; Wang, H.; Chung, C.; Lopreiato, N. P.; Sweeny, E. A.; Knight, M. N.; Shorter, J. *Nat. Chem. Biol.* **2009**, *5*, 936−946.
(28) Bieschke, J.; Russ, J.; Friedrich, R. P.; Ehrnhoefer, D. E.; Wobst, H.; Neugebauer, K.; Wanker, E. E. *Proc. Natl. Acad. Sci. U.S.A.* **2010**, *107*, 7710−7715.
(29) Ehrnhoefer, D. E.; Bieschke, J.; Boeddrich, A.; Herbst, M.; Masino, L.; Lurz, R.; Engemann, S.; Pastore, A.; Wanker, E. E. *Nat. Struct. Biol.* **2008**, *15*, 558−566.
(30) Meng, F.; Abedini, A.; Plesner, A.; Verchere, C. B.; Raleigh, D. P. *Biochemistry* **2010**, *49*, 8127−8133.
(31) Sinha, S.; Du, Z.; Maiti, P.; Klärner, F.-G.; Schrader, T.; Chunyu Wang; Bitan, G. *ACS Chem. Neurosci.* **2012**, *3*, 451−458.
(32) McLaurin, J.; Golomb, R.; Jurewicz, A.; Antel, J. P.; Fraser, P. E. *J. Biol. Chem.* **2000**, *275*, 18495−18502.
(33) Bourgault, S.; Solomon, J. P.; Reixach, N.; Kelly, J. W. *Biochemistry* **2011**, *50*, 1001−1015.
(34) Motamedi-Shad, N.; Monsellier, E.; Torrassa, S.; Relini, A.; Chiti, F. *J. Biol. Chem.* **2009**, *284*, 29921−29934.
(35) Vilasi, S.; Sarcina, R.; Maritato, R.; Simone, A. D.; Irace, G.; Sirangelo, I. *PLoS One* **2011**, *6*, e22076.
(36) Cohlberg, J. A.; Li, J.; Uversky, V. N.; Fink, A. L. *Biochemistry* **2002**, *41*, 1502−1511.
(37) Kanekiyo, T.; Zhang, J.; Liu, Q.; Liu, C.-C.; Zhang, L.; Bu, G. *J. Neurosci.* **2011**, *31*, 1644−1651.
(38) Madine, J.; Middleton, D. A. *Eur. Biophys. J.* **2010**, *39*, 1281−1288.
(39) Bazar, E.; Jelinek, R. *ChemBioChem* **2010**, *11*, 1997−2002.
(40) Capila, I.; Linhardt, R. J. *Angew. Chem., Int. Ed.* **2002**, *41*, 390−412.

(41) Petkova, A. T.; Leapman, R. D.; Guo, Z.; Yau, W.-M.; Mattson, M. P.; Tycko, R. *Science* **2005**, *307*, 262−265.
(42) Campioni, S.; Mannini, B.; Zampagni, M.; Pensalfini, A.; Parrini, C.; Evangelisti, E.; Relini, A.; Stefani, M.; MDobson, C.; Cecchi, C.; Chiti, F. *Nat. Chem. Biol.* **2010**, *6*, 140−147.
(43) Bleiholder, C.; Dupuis, N. F.; Wyttenbach, T.; Bowers, M. T. *Nat. Chem.* **2011**, *3*, 172−177.
(44) Teplow, D. B.; Lazo, N. D.; Bitan, G.; Bernstein, S.; Wyttenbach, T.; Bowers, M. T.; Baumketner, A.; Shea, J.-E.; Urbanc, B.; Cruz, L.; Borreguero, J.; Stanley, H. E. *Acc. Chem. Res.* **2006**, *39*, 635−645.
(45) Dupuis, N. F.; Wu, C.; Shea, J.-E.; Bowers, M. T. *J. Am. Chem. Soc.* **2011**, *133*, 7240−7243.
(46) Dupuis, N. F.; Wu, C.; Shea, J. E.; Bowers, M. T. *J. Am. Chem. Soc.* **2009**, *131*, 18283−18292.
(47) von Helden, G.; Wyttenbach, T.; Bowers, M. T. *Science* **1995**, *267*, 1483−1485.
(48) von Helden, G.; Gotts, N. G.; Bowers, M. T. *Nature* **1993**, *363*, 60−63.
(49) Bowers, M. T.; Kemper, P. R.; von Helden, G.; van Koppen, P. A. M. *Science* **1993**, *260*, 1446−1451.
(50) Ruotolo, B. T.; Giles, K.; Campuzano, I.; Sandercock, A. M.; Bateman, R. H.; Robinson, C. V. *Science* **2005**, *310*, 1658−1661.
(51) Kubo, T.; Nishimura, S.; Kumagae, Y.; Kaneko, I. *J. Neurosci. Res.* **2002**, *70*, 474−483.
(52) Loo, D. T.; Copani, A.; Christian, J. Pike; Whittemore, E. R.; Walencewicz, A. J.; Cotman, C. W. *Proc. Natl. Acad. Sci. U.S.A.* **1993**, *90*, 7951−7955.
(53) Pike, C. J.; Walencewicz-Wasserman, A. J.; Kosmoski, J.; Cribbs, D. H.; Glabe, C. G.; Cotman, C. W. *Journal of Neurochemistrv* **1995**, *64*, 253−265.
(54) Frozza, R. L.; Horn, A. P.; Hoppe, J. B.; Simao, F.; Gerhardt, D.; Comiran, R. A.; Salbego, C. G. *Neurochem. Res.* **2009**, *34*, 295−303.
(55) Zameer, A.; Schulz, P.; Wang, M. S.; Sierks, M. R. *Biochemistry* **2006**, *45*, 11532−11539.
(56) Wei, G.; Jewett, A. I.; Shea, J.-E. *Phys. Chem. Chem. Phys.* **2010**, *12*, 3622−3629.
(57) Wei, G.; Shea, J.-E. *Biophys. J.* **2006**, *91*, 1638−1647.
(58) Kittner, M.; Knecht, V. *J. Phys. Chem. B* **2010**, *114*, 15288−15295.
(59) Larini, L.; Shea, J.-E. *Biophys. J.* **2012**, *103*, 576−586.
(60) Bastianetto, S.; Yao, Z. X.; Papadopoulos, V.; Quirion, R. *Eur. J. Neurosci.* **2006**, *23*, 55−64.
(61) Pringle, S. D.; Giles, K.; Wildgoose, J. L.; Williams, J. P.; Slade, S. E.; Thalassinos, K.; Bateman, R. H.; Bowers, M. T.; Scrivens, J. H. *Int. J. Mass Spectrom.* **2007**, *261*, 1−12.
(62) Colletier, J. P.; Laganowsky, A.; Landau, M.; Zhao, M.; Soriaga, A. B.; Goldschmid, t. L.; Flot, D.; Cascio, D.; Sawaya, M. R.; Eisenberg, D. *Proc. Natl. Acad. Sci. U.S.A.* **2011**, *108*, 16938−16943.
(63) Liu, F.-F.; Dong, X.-Y.; He, L.; Middelberg, A. P. J.; Sun, Y. *J. Phys. Chem. B* **2011**, *115*, 11879−11887.
(64) Nelson, R.; Sawaya, M. R.; Balbirnie, M.; Madsen, A. Ø.; Riekel, C.; Grothe, R.; Eisenberg, D. *Nature* **2005**, *435*, 773−778.
(65) Shima, S.-H.; Guptab, R.; Linga, Y. L.; Strasfelda, D. B.; Raleigh, D. P.; Zannia, M. T. *Proc. Natl. Acad. Sci. U.S.A.* **2009**, *106*, 6614−6619.
(66) Wiltzius, J. J. W.; Sievers, S. A.; Sawaya, M. R.; Cascio, D.; Popov, D.; Riekel, C.; Eisenberg, D. *Protein Sci.* **2008**, *17*, 1467−1474.
(67) Sawaya, M. R.; Sambashivan, S.; Nelson, R.; Ivanova, M. I.; Sievers, S. A.; Apostol, M. I.; Thompson, M. J.; Balbirnie, M.; Wiltzius, J. J. W.; MacFarlane, H. T.; Madsen, A. Ø.; Riekel, C.; Eisenberg, D. *Nature* **2007**, *447*, 453−457.
(68) Knowles, T. P. J.; Smith, J. F.; Devlin, G. L.; Dobson, C. M.; Welland, M. E. *Nanotechnology* **2007**, *18*, 1−5.
(69) Eichner, T.; Kalverda, A. P.; Thompson, G. S.; Homans, S. W.; Radford, S. E. *Mol. Cell* **2011**, *41*, 161−172.
(70) Sievers, S. A.; Karanicolas, J.; Chang, H. W.; Zhao, A.; Jiang, L.; Zirafi, O.; Stevens, J. T.; Münch, J.; Baker, D.; Eisenberg, D. *Nature* **2011**, *475*, 96−100.
(71) Grill, J. D.; Cummings, J. L. *Exp. Rev. Neurother.* **2010**, *10*, 711−728.
(72) Chang, Z.; Luo, Y.; Zhang, Y.; Wei, G. *J. Phys. Chem. B* **2011**, *115*, 1165−1174.
(73) Li, G.; Rauscher, S.; Baud, S.; Pomès, R. *J. Phys. Chem. B* **2012**, *116*, 1111−1119.
(74) Kemper, P. R.; Dupuis, N. F.; Bowers, M. T. *Int. J. Mass Spectrom.* **2009**, *287*, 46−57.
(75) Wang, J. M.; Wolf, R. M.; Caldwell, J. W.; Kollman, P. A.; Case, D. A. *J. Comput. Chem.* **2004**, *25*, 1157−1174.
(76) Duan, Y.; Chowdhury, S.; Xiong, G.; Wu, C.; Zhang, W.; Lee, T.; Cieplak, P.; Caldwell, J.; Luo, R.; Wang, J.; Kollman, P. A. *J. Comput. Chem.* **2003**, *24*, 1999−2012.
(77) Case, D. A.; Darden, T. A.; T.E. Cheatham, I.; Simmerling, C. L.; Wang, J.; Duke, R. E.; Luo, R.; Merz, K. M.; Wang, B.; Pearlman, D. A.; Crowley, M.; Brozell, S.; Tsui, V.; Gohlke, H.; Mongan, J.; Hornak, V.; Cui, G.; Beroza, P.; Schafmeister, C.; Caldwell, J. W.; Ross, W. S.; Kollman, P. A.; *Amber Molecular Dynamics*; University of California: San Francisco, 2004.
(78) Mesleh, M. F.; Hunter, J. M.; Shvartsburg, A. A.; Schatz, G. C.; Jarrold, M. F. *J. Phys. Chem. A* **1996**, *100*, 16082−16086.
(79) Bleiholder, C.; Wyttenbach, T.; Bowers, M. T. *Int. J. Mass Spectrom.* **2011**, *308*, 1−10.
(80) Anderson, S. E.; Bleiholder, C.; Brocker, E. R.; Stang, P. J.; Bowers, M. T. *Int. J. Mass Spectrom.* **2012**, *330*−*332*, 78−84.
(81) Bleiholder, C.; Contreras, S.; Do, T. D.; Bowers, M. T. *Int. J. Mass Spectrom.* **2013**, *345*−*347*, 89−96.